Gas-phase epitaxy grown InP(001) surfaces from real-space finite-difference calculations

W.G. Schmidt, P.H. Hahn, K. Seino, M. Preuß, and F. Bechstedt

Computational Materials Science Group
Institut für Festkörpertheorie und Theoretische Optik
Friedrich-Schiller-Universität, Max-Wien-Platz 1, 07743 Jena
http://www.ifto.uni-jena.de/en/begin.html

Summary. Density-functional calculations based on finite-difference discretization and multigrid acceleration are used to explore the atomic and spectroscopic properties of P-rich InP(001)(2×1) surfaces grown in gas-phase epitaxy. These surfaces have been reported to consist of a semiconducting monolayer of buckled phosphorus dimers. This apparent violation of the electron counting principle was explained by effects of strong electron correlation. Our calculations show that the (2×1) reconstruction is not at all a clean surface: it is induced by hydrogen adsorbed in an alternating sequence on the buckled P-dimers. Thus, the microscopic structure of the InP growth plane relevant to standard gas-phase epitaxy conditions is resolved and shown to obey the electron counting rule.

1 Introduction

The most widely used numerical discretization methods to solve the equations of density-functional theory (DFT) are linear combination of atomic orbitals (LCAO), plane-waves (PW) and finite differences (FD). Of these three, FD is the most recent method. Fully three-dimensional grid-based electronic structure representations using finite differences as approximate numerical scheme for partial differential operators have started being widely used in the last ten years only. Traditionally, chemists have mostly used LCAO methods. Atomic orbitals expressed as linear combinations of Gaussian functions allow for a numerically very efficient description of the electronic structure of localized systems such as molecules. This is exploited in the wide spread commercial code GAUSSIAN. Plane waves, on the other hand, efficiently describe systems characterized by periodic boundary conditions [1]. Because plane waves are eigenfunctions of the momentum operator, the PW approach has been most successful at describing systems with almost free electrons, such as metals. By its nature, the PW method has mainly been developed and used by condensed matter physicists. In this approach, known as pseudo-spectral method

in the mathematics community, the numerical basis set is completely independent of the positions of the atoms present in the simulation. It can be made as accurate as desired by systematically increasing the number of basis functions. Similarly, the finite-difference method is an alternative to the linear combination of atomic orbitals when highly accurate electronic wave functions are required. No assumption on where the atoms and electrons are located is made. In recent years, large parallel supercomputers have become an essential tool in *first-principles* molecular dynamics simulations. They not only allow for calculations to be completed within hours or days that would take months or years to be completed on single processor machines, but also for calculations that would just not fit into the memory of a workstation or personal computer. In a parallel environment, the electronic wave functions described in a PW approach are usually distributed between the processors. Every time a matrix element between two wave functions is required, a considerable data traffic through the whole machine is necessary. In a real-space FD approach, all the expensive operations can be done locally, thanks to the real-space nature of the DFT Hamiltonian. To compute matrix elements between wave functions, local contributions are computed on every processor before being summed up globally at the end. This is one of the main advantages of FD over PW for nowadays simulations. It has been exploited extensively by our group in the context of developing codes which allow for the efficient calculation of many-body effects in excitation spectra [2, 3, 4]. Furthermore, large-scale real-space calculations involve large sparse matrices, and multigrid methods [5], either as solvers or preconditioners, allow to design very efficient scalable algorithms [6, 7, 8]. More recently, in the context of the search for linear scaling algorithms, real-space methods have appeared to be appropriate for imposing natural localization constraints on the orbitals [9]. Such an approach leads to a dramatic reduction in computer time and memory requirements for very large systems. Other advantages of FD over standard PW approaches include the possibility of introducing local mesh refinements [10] and Dirichlet boundary conditions in a natural fashion.

Advanced numerical methods such as discussed above are useful only if they allow for treating real-world problems. One such problem is the accurate determination of the atomic and electronic structure of semiconductor growth planes. While the properties of clean surfaces under ultrahigh vacuum (UHV) conditions are reasonably well understood, very little is known about the structure of surfaces under growth conditions. In the present article we clarify the hitherto open structure of the gas-phase grown InP(001)(2×1) surface by means of accurate total-energy and electronic structure calculations based on a FD scheme [8]. To our knowledge, this is the first example of an atomically resolved gas-phase epitaxy growth structure.

The ideal III-V(001) surface is polar, being terminated either entirely by cations or anions. However, such an ideal termination is usually not observed [11, 12, 13]. InP(001) seems to be a remarkable exception in that respect. For specific P-rich preparation conditions it is apparently terminated by a com-

plete phosphorus monolayer, forming a nominal (2×1) reconstructed surface [14, 15]. Such a structure clearly violates the electron counting rule [16] and should be metallic. However, in this case an energy gap between valence and conduction states of more than one eV was measured. The formation of this unusual surface structure and the band gap were explained by strong electron correlation effects between the P dangling bonds across the dimer rows [14]. As a result, the P dimers buckle and form zig-zag chains along the [110] direction. Zig-zag chains are indeed clearly resolved by scanning tunneling microscopy (STM) [14, 15]. Depending on whether two adjacent chains are in or out of phase, (2×2) and $c(4\times2)$ reconstructed domains, reminiscent of the Si(001) surface, are observed.

Such observations, however, have exclusively been made by groups using metal-organic vapor phase epitaxy (MOVPE) and chemical beam epitaxy (CBE) to prepare their InP samples [14, 15, 17, 18, 19]. Samples prepared by molecular beam epitaxy (MBE) show only two reconstructions with long range periodicity, $c(4\times4)$ and (2×4) [20, 21]. On the other hand, to our knowledge the $c(4\times4)$ surface has never been observed on gas-source grown samples. The MBE results agree with total-energy calculations [13], which identified several stable surface geometries with (2×4) and $c(4\times4)$ periodicity. An extensive computational search for geometries able to explain the peculiar (2×1) surface ordering failed [22]. Symmetric, rather than asymmetric P dimers were found to be energetically favored.

A solution of this puzzle is highly desirable: gas-phase epitaxy is an essential technology for manufacturing compound semiconductor devices, in particular those containing phosphide-based materials. The microscopic understanding of surfaces prepared by MOVPE or CBE is the prerequisite for any reliable computational modeling of the complex transport and reaction phenomena during the epitaxial growth. In the present study we explore the possibility that the apparent discrepancies between the outcome of gas-phase epitaxy and MBE experiments can be explained by the presence of hydrogen in the former case: While hydrogen is present in MOVPE and CBE, it is absent under MBE conditions. Furthermore, hydrogen is difficult to detect. It may thus be the key to resolve the puzzle of the (2×1) surface.

2 Computational Method

Our calculations are based on density-functional theory [23] which states that the electronic ground state of a physical system can be described by a system of orthogonal one-particle electronic wave functions $\psi_j, j = 1, ..., N$ that minimizes the Kohn-Sham total-energy functional

$$E_{KS}[\{\psi_i\}_{i=1}^{N},\{\mathbf{R}\}_{\alpha=\mathbf{1}}^{\mathbf{N}_\alpha}] = \sum_{i=1}^{N} f_i \int_\Omega \psi_i^*(\mathbf{r})(-\frac{1}{2}\nabla^2)\psi_i(\mathbf{r})d\mathbf{r} \quad (1)$$
$$+\frac{1}{2}\int_\Omega\int_\Omega \frac{\rho_e(\mathbf{r}')\rho_e(\mathbf{r}'')}{|\mathbf{r}'-\mathbf{r}''|}d\mathbf{r}'d\mathbf{r}'' + E_{XC}[\rho_e],$$
$$+\int_\Omega \psi_i^*(\mathbf{r})(V_{ext}\psi_i)(\mathbf{r})d\mathbf{r}$$

where N_α atoms are located at $\{\mathbf{R}\}_{\alpha=\mathbf{1}}^{\mathbf{N}_\alpha}$, and the electronic density is given by

$$\rho_e(\mathbf{r}) = \sum_{i=1}^{N} f_i|\psi_i(\mathbf{r})|^2 \ , \quad (2)$$

with $0 \le f_i \le 2$ being the occupation numbers. E_{XC} models the exchange and correlation between electrons. Here we use the local density approximation (LDA) in the parameterization of Ref. [24]. The minimum of the energy functional (1) can be found by solving the associated Euler-Lagrange (or Kohn-Sham) equations [25]

$$H\psi_j = \left\{-\frac{1}{2}\nabla^2 + v_H(\rho_e) + \mu_{XC}(\rho_e) + V_{ext}\right\}\psi_j = \epsilon_j\psi_j \quad (3)$$

self-consistently for the N lowest eigenvalues ϵ_j, while imposing the orthonormality constraints $\langle\psi_j|\psi_i\rangle = \delta_{ji}$. The Hartree potential v_H represents the Coulomb potential due to the electronic charge density ρ_e, and $\mu_{XC} = \delta E_{XC}[\rho_e]/\delta\rho_e$ is the exchange and correlation potential. In order to discretize the Kohn-Sham equations, a real-space rectangular grid Ω_h of mesh spacing h_x, h_y, h_z in the x, y, and z directions is introduced, covering the computation domain Ω. Let M be the number of grid points. The wave functions, potentials and the electronic density are represented by their values at the grid points $\mathbf{r}_{ijk}$. Integrals over Ω are performed using the discrete summation rule

$$\int_\Omega u(\mathbf{r})d\mathbf{r} \approx h_x h_y h_z \sum_{i,j,k\in\Omega_h} u(\mathbf{r}_{ijk}) \ . \quad (4)$$

Given the values of a function $u(\mathbf{r})$ on a set of nodes $\mathbf{r}_{ijk}$, the traditional FD approximation $w_{i,j,k}$ to the Laplacian of the function at a given node is expressed as a linear combination of values of the function at the neighboring nodes

$$w_{i,j,k} = \sum_{n=-p}^{p} c_n(u(x_i+nh_x, y_j, z_k) + u(x_i, y_j+nh_y, z_k) + u(x_i, y_j, z_k+nh_z)) \quad (5)$$

where the coefficients $\{c_n\}$ can be computed from the Taylor expansion of u near $\mathbf{r}_{ijk}$. Such an approximation has an order of accuracy $2p$, that is for a sufficiently smooth function u, $w_{i,j,k}$ will converge at the rate $\mathcal{O}(h^{2p})$ as the mesh

spacing $h \longrightarrow 0$. For the second order approximation for example ($p = 1$), we have $c_0 = 2/h^2$ and $c_1 = -1/h^2$. High order versions of this scheme were first introduced in electronic structure calculations by Chelikowski and co-workers [26]. In the present work we use an alternative, compact FD scheme called *Mehrstellenverfahren* [27]. In contrast to the central difference approximation, this discretization uses more *local* information. The fourth-order *Mehrstellen* discretization leads to an eigenvalue problem of the form

$$\left\{\frac{1}{2}L_h + B_h V_h\right\}\psi_i = \epsilon_i B_h \psi_i \tag{6}$$

for the Kohn-Sham equations (3) with operators defined by

$$L_h u(\mathbf{r}) = \frac{4}{h^2}u(\mathbf{r}_0) - \frac{1}{3h^2}\sum_{\substack{r\in\Omega_h \\ |\mathbf{r}-\mathbf{r}_0|=h}} u(\mathbf{r}) - \frac{1}{6h^2}\sum_{\substack{r\in\Omega_h \\ |\mathbf{r}-\mathbf{r}_0|=\sqrt{2}h}} u(\mathbf{r}) \tag{7}$$

$$B_h u(\mathbf{r}) = \frac{1}{2}u(\mathbf{r}_0) + \frac{1}{12}\sum_{\substack{r\in\Omega_h \\ |\mathbf{r}-\mathbf{r}_0|=h}} u(\mathbf{r}). \tag{8}$$

For simplicity, we have assumed here that $h_x = h_y = h_z$, but this expression is easily generalized [7]. This scheme requires only values at grid points within a sphere of radius $\sqrt{2}h$. Besides its good numerical properties (see, e.g. Ref. [7]), its compactness reduces the amount of communication in a domain-decomposition based parallel implementation compared to traditional FD approximations.

This scheme was introduced in electronic structure calculations by Briggs *et al.* [6] and Fattebert [28]. To efficiently solve (6), we use multigrid iteration techniques that accelerate convergence by employing a sequence of grids of varying resolutions. The final solution is obtained on a grid fine enough to accurately represent the potential and wave functions. This procedure provides excellent preconditioning for all length scales present in the system and leads to very rapid convergence rates. The operation count to converge one wave function with a fixed potential is $\mathcal{O}(M)$, compared to $\mathcal{O}(M \log M)$ for PW approaches.

The InP(001) surface structures studied in the following were modeled using periodic supercells. They contain material slabs of 16 InP(001) layers, separated by vacuum regions large enough to decouple the surfaces. This corresponds to a grid of $M = 32 \times 32 \times 144$ points. Between $170 - 270$ wave functions were included in the calculations. The real-space grid was mapped on $64 - 256$ Cray T3E processors. Parallelizing is done using Message Passing Interface (MPI). Earlier we have shown the excellent scaling behaviour of this method using up to 512 Cray T3E processors (Fig. in 1 in Ref. [29]). Typical job run times amount to $4 - 12$ wall clock hours.

The possibility of hydrogen adsorption on gas-phase grown InP surfaces leads to a large number of conceivable structures. We investigate more than

50 models, which differ with respect to their geometries, their In/P ratio, and the number of adsorbed hydrogen atoms. The energetically favored hydrogen-induced surface reconstructions are shown in Fig. 1. The notation of surface structures is chosen such that a leading P indicates adsorption on top of a P-terminated substrate and a hyphen followed by P, D or MD denotes adsorption of P atoms, P dimers or mixed In-P dimers, respectively. The number of hydrogens per surface unit cell concludes the notation.

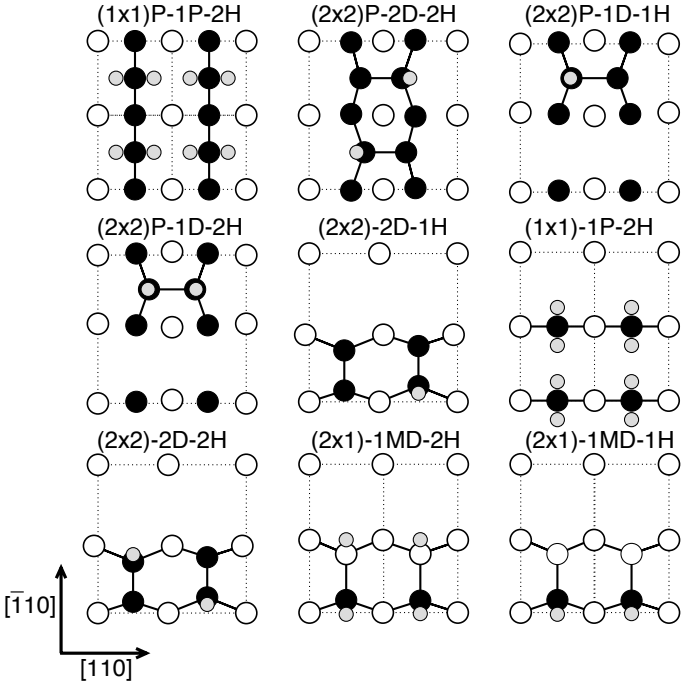

Fig. 1. Top view of relaxed InP(001):H surface structures. Empty (filled,grey) circles represent In (P, H) atoms. The surface unit cells are indicated.

Due to the varying surface stoichiometry, the total energies of the studied structures cannot directly be used to determine the surface ground state. Rather, the thermodynamic grandcanonical potential Ω in dependence on the chemical potentials μ of In, P and H needs to be considered. Since the surface is in equilibrium with the bulk compound, μ_{In} and μ_P are related to each other: their sum equals the chemical potential of bulk InP. Consequently, the surface formation energy may be written as a function of only two variables, which we take to be the relative chemical potential of indium with respect to its bulk phase and the chemical potential of hydrogen with respect to its molecular phase. The computational accuracy in determining the chemical potentials is of the order of 0.1 eV [30]. From convergence tests, the uncertainty of the

calculated surface energies is estimated to be smaller than 0.01 eV per surface atom.

3 Results

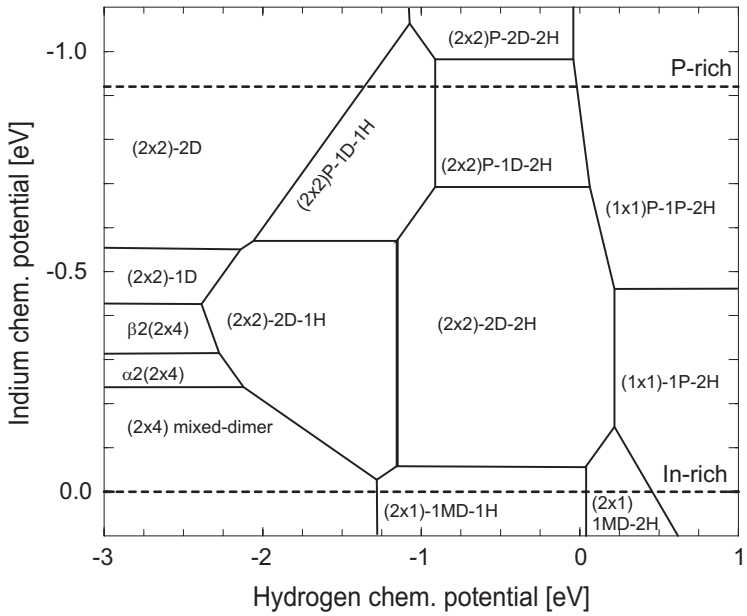

Fig. 2. Calculated phase diagram of the hydrogen-exposed InP(001) surface. Dashed lines indicate the approximate range of the thermodynamically allowed values of the In chemical potential. The chemical potential of hydrogen is given with respect to molecular hydrogen at $T = 0$ K.

The calculated surface phase diagram in terms of its dependence on the chemical potentials of In and H is shown in Fig. 2. Here zero hydrogen chemical potential corresponds to the situation where the surface is exposed to molecular hydrogen at $T = 0$ K. For higher temperatures the surface phase diagram will change, due to vibrational contributions to the energy and entropy of the surface structures, and due to the temperature (and pressure) dependence of the chemical potentials of the surface constituents. By far the largest change of the surface energetics, however, is related to the hydrogen chemical potential. The temperature and pressure dependence of $\Delta\mu_H$ can be approximated by that of a two-atomic ideal gas [31].

$$\Delta\mu_H(T) = \frac{1}{2}kT\left\{\ln(\frac{p\lambda^3}{kT}) - \ln Z_{rot} - \ln Z_{vib}\right\}, \tag{9}$$

where k is the Boltzmann constant, T is the temperature, p the pressure, $\lambda = (\frac{h^2}{2\pi mkT})^{1/2}$ the de Broglie thermal wavelength of the H_2 molecule, and Z_{rot} and Z_{vib} its rotational and vibrational partition functions, respectively. By increasing the temperature, the hydrogen chemical potential is lowered, i.e., less energy is gained by taking a H atom out of the reservoir and attaching it to the InP surface. In Fig. 3 we show the temperature and pressure values corresponding to specific values for $\Delta\mu_H(T)$. A hydrogen chemical potential $\Delta\mu$(H) of about -1 eV can be estimated to correspond to typical MOVPE growth conditions.

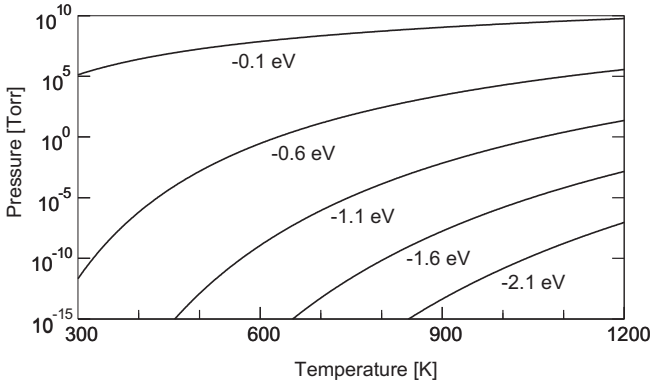

Fig. 3. Temperature and pressure values corresponding to given relatives change of the hydrogen chemical potential with respect to its molecular value at T = 0 K.

The structures indicated for $\Delta\mu_H > 0$ in the phase diagram of Fig. 2 may form when atomic hydrogen becomes available for the surface reaction. In that case the reaction barrier is also substantially lowered. If no hydrogen is present, i.e. for $\Delta\mu_H \ll 0$, InP forms the surface reconstructions typical for the clean surface [13]. The $c(4\times4)$ reconstruction, not visible in the present phase diagram, is energetically nearly degenerate with other P-rich surface reconstructions. It is stable for a narrow range of $\Delta\mu_{In}$ between the (2×2)-2D and (2×2)-1D surfaces.

The (2×2)-2D-2H surface is the most dominant structure in the calculated surface phase diagram in Fig. 2. It should occur for a wide range of surface preparation conditions. It is formed by a periodic arrangement of oppositely buckled (Δz = 0.30 Å) P dimers on top of an In-terminated substrate. One H atom is bonded to the "down" atom of the P dimer (cf. Fig. 1). While this structure seems to represent the surface ground state for annealed gas-phase epitaxy grown InP(001) surfaces, energetical arguments alone are only an indication that this structure indeed corresponds to the surface observed experimentally [14, 15], because its formation may be kinetically hindered.

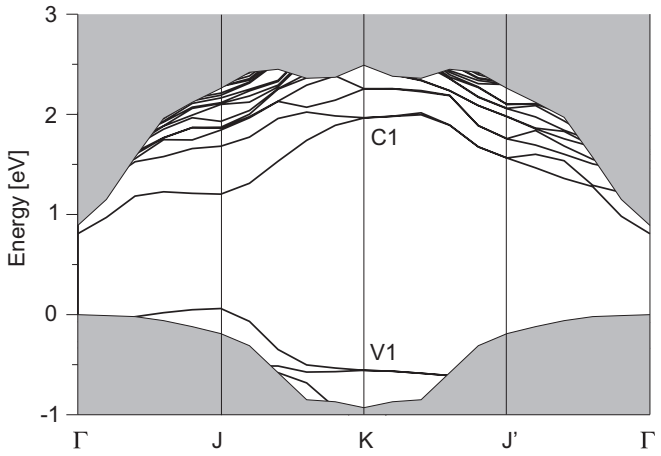

Fig. 4. Surface band structure for the (2x2)-2D-2H surface. Grey regions indicate the projected bulk band structure.

In order to clarify whether the 2D-2H structure indeed corresponds to the experimental observations, we investigate its electronic structure. The model obeys the electron counting rule. Its surface bands calculated along the high-symmetry lines of the (2×2) surface Brillouin zone are shown in Fig. 4. The surface band gap calculated in DFT-LDA amounts to 0.75 eV. This value is lower than the one measured for the zig-zag chain structure of 1.2 ± 0.2 eV [14]. This discrepancy, however, can be explained by the insufficient description of the electronic self-energy within the DFT-LDA [32]. The inclusion of quasiparticle effects results in an opening of the InP(001) surface band gap by about $0.4 - 0.5$ eV [33].

The highest occupied surface band, V1, is due to the dangling bonds on the "up" atoms of the Phosphorus dimers. The lowest unoccupied surface band, C1, is related to an antibonding σ^* combination of in-plane p orbitals localized at the P dimer atoms (cf. Fig. 5).

In Fig. 6 we show a STM image of the (2x2)-2D-2H surface, calculated according to the Tersoff-Hamann approach [34]. A bias voltage of -5 eV was used, to allow for a meaningful comparison with the experiments of Refs. [14, 15]. Clearly, the simulated STM image is in very good agreement with the measured data (cf., e.g., Fig. 2 of Ref. [14]). The bright spots visible in the image are due mainly to the dangling bonds at the "up" atom of the P dimer, i.e., the V1 surface state. The alternating arrangement of the dangling bonds causes the appearance of zig-zag chains in the STM. By varying the phase shift between adjacent zig-zag chains, the observation of (2×2) and $c(4\times2)$ reconstructed domains can be explained.

We mention that experimental evidence for the existence of hydrogen at annealed, MOVPE-grown InP(001)(2×1) surfaces has recently been obtained

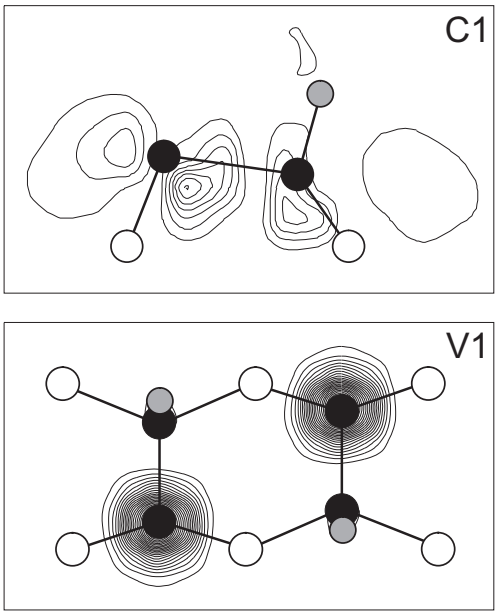

Fig. 5. Contour plots of the squared wave functions of the (2x2)-2D-2H surface at the K point of the (2×2) surface Brillouin zone. Top and side views are given for V1 and C1, respectively.

by optical spectroscopy. The comparison between the calculated and measured surface optical response [35] lends further credibility to the 2D-2H structure predicted here.

4 Conclusions

In conclusion, we performed large-scale real-space finite-difference calculations for a large variety of clean and H-covered InP(001) surfaces. Oppositely buckled P dimers with one hydrogen adsorbed are energetically favored for a wide range of the surface chemical potentials. The simulated STM image as well as the calculated surface band gap for this structure agree very well with the experimental findings obtained for P monolayer-terminated InP(001) surfaces prepared by the annealing of gas-phase epitaxy grown samples. The adsorption of hydrogen thus provides a simple explanation, as opposed to electron-correlation effects, for the experimental observation of a Si(001)-like surface ordering and the existence of a band gap. Our results underline the strong influence of the surface preparation procedures on the geometries finally obtained. In particular the importance of adsorbates resulting from decomposition products of precursors on the microscopic structure of gas-phase epitaxy grown surfaces has been demonstrated.

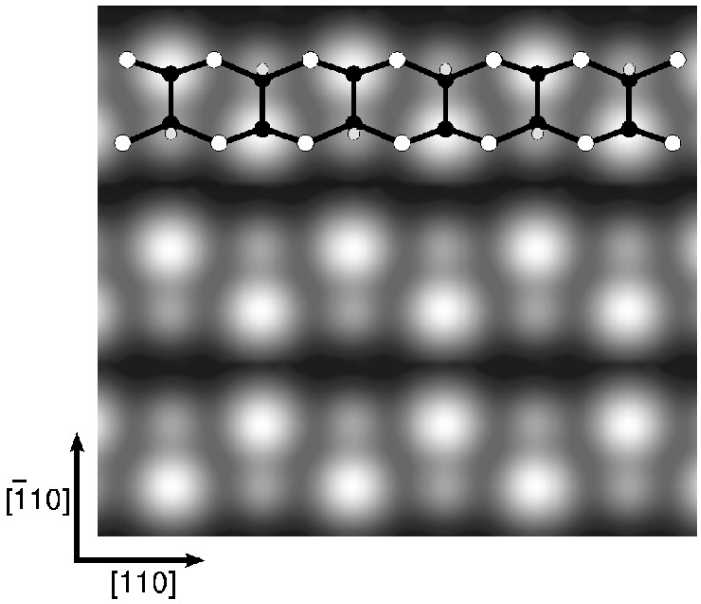

Fig. 6. STM image calculated for the (2x2)-2D-2H surface.

Acknowledgments

We thank Norbert Esser, Patrick Vogt, Wolfgang Richter, Lars Töben and Frank Willig for stimulating discussions on the growth of III-V compound semiconductors. Jean-Luc Fattebert, Emil Briggs and Jerry Bernholc are acknowledged for their help concerning the numerical and computational aspects of this work. Generous grants of computer time from the the Höchstleistungsrechenzentrum Stuttgart and the Leibniz-Rechenzentrum München made the calculations possible.

References

1. M. C. Payne, M. P. Teter, D. C. Allan, T. A. Arias, and J. D. Joannopoulos, Rev. Mod. Phys. **64**, 1045 (1992).
2. W. G. Schmidt, J. L. Fattebert, J. Bernholc, and F. Bechstedt, Surf. Rev. Lett. **6**, 1159 (1999).
3. P. H. Hahn, W. G. Schmidt, and F. Bechstedt, Phys. Rev. Lett. **88**, 016402 (2002).
4. W. G. Schmidt, S. Glutsch, P. H. Hahn, and F. Bechstedt, Phys. Rev. B **67**, 085307 (2003).
5. A. Brandt, Math. Comp. **31**, 333 (1977).
6. E. L. Briggs, D. J. Sullivan, and J. Bernholc, Phys. Rev. B **52**, R5471 (1995).
7. E. L. Briggs, D. J. Sullivan, and J. Bernholc, Phys. Rev. B **54**, 14362 (1996).

8. J. Bernholc, E. L. Briggs, C. Bungaro, M. B. Nardelli, J. L. Fattebert, K. Rapcewicz, C. Roland, W. G. Schmidt, and Q. Zhao, phys. stat. sol. (b) **217**, 685 (2000).
9. J. L. Fattebert and J. Bernholc, Phys. Rev. B **62**, 1713 (2000).
10. J. L. Fattebert, J. Comput. Phys. **149**, 75 (1999).
11. W. Mönch, *Semiconductor Surfaces and Interfaces* (Springer-Verlag, Berlin, 1995).
12. Q.-K. Xue, T. Hashizume, and T. Sakurai, Prog. Surf. Sci. **56**, 1 (1997).
13. W. G. Schmidt, Appl. Phys. A **75**, 89 (2002).
14. L. Li, B.-K. Han, Q. Fu, and R. F. Hicks, Phys. Rev. Lett. **82**, 1879 (1999).
15. P. Vogt, T. Hannappel, S. Visbeck, K. Knorr, N. Esser, and W. Richter, Phys. Rev. B **60**, R5117 (1999).
16. M. D. Pashley, Phys. Rev. B **40**, 10481 (1989).
17. L. Li, B.-K. Han, D. Law, C. H. Li, Q. Fu, and R. F. Hicks, Appl. Phys. Lett. **683**, 75 (1999).
18. L. Li, Q. Fu, C. H. Li, B.-K. Han, and R. F. Hicks, Phys. Rev. B **61**, 10223 (2000).
19. B. X. Yang and H. Hasegawa, Jpn. J. Appl. Phys. **33**, 742 (1994).
20. K. B. Ozanyan, P. J. Parbrook, M. Hopkinson, C. R. Whitehouse, Z. Sobiesierski, and D. I. Westwood, J. Appl. Phys. **82**, 474 (1997).
21. V. P. LaBella, Z. Ding, D. W. Bullock, C. Emery, and P. M. Thibado, J. Vac. Sci. Technol. A **18**, 1492 (2000).
22. O. Pulci, K. Lüdge, W. G. Schmidt, and F. Bechstedt, Surf. Sci. **464**, 272 (2000).
23. P. Hohenberg and W. Kohn, Phys. Rev. **136**, B864 (1964).
24. J. P. Perdew and A. Zunger, Phys. Rev. B **23**, 5048 (1981).
25. W. Kohn and L. J. Sham, Phys. Rev. **140**, A1133 (1965).
26. J. R. Chelikowski, N. Troullier, and Y. Saad, Phys. Rev. Lett. **72**, 1240 (1994).
27. L. Collatz, *The Numerical Treatment of Differential Equations* (Springer-Verlag, Berlin, 1966).
28. J. L. Fattebert, BIT **36**, 509 (1996).
29. W. G. Schmidt, P. H. Hahn, and F. Bechstedt, in *High Performance Computing in Science and Engineering 2001* (Springer-Verlag, Berlin, 2002), Chap. GaAs and InAs(001) Surface Structures from Large-scale Real-space Multigrid Calculations, p. 178.
30. W. G. Schmidt, Appl. Phys. A **65**, 581 (1997).
31. L. D. Landau and E. M. Lifshitz, *Lehrbuch der Theoretischen Physik* (Akademie-Verlag, Berlin, 1987), Vol. 5.
32. F. Bechstedt, in *Festköperprobleme / Advances in Solid State Physics*, edited by U. Rössler (Vieweg, Braunschweig/Wiesbaden, 1992), Vol. 32, p. 161.
33. W. G. Schmidt, N. Esser, A. M. Frisch, P. Vogt, J. Bernholc, F. Bechstedt, M. Zorn, T. Hannappel, S. Visbeck, F. Willig, and W. Richter, Phys. Rev. B. **61**, R16335 (2000).
34. J. Tersoff and D. R. Hamann, Phys. Rev. B **31**, 805 (1985).
35. W. G. Schmidt, P. H. Hahn, F. Bechstedt, N. Esser, P. Vogt, A. Wange, and W. Richter, Phys. Rev. Lett. **90**, 126101 (2003).